



International Journal of Orthopaedics Sciences

E-ISSN: 2395-1958
P-ISSN: 2706-6630
IJOS 2019; 5(4): 652-661
© 2019 IJOS
www.orthopaper.com
Received: 04-08-2019
Accepted: 08-09-2019

Dr. AN Mishra
Professor, Department of
Orthopaedics, Era's Lucknow
Medical College, Lucknow, Uttar
Pradesh, India

Dr. Shakeel A Qidwai
Professor, Department of
Orthopaedics, Era's Lucknow
Medical College, Lucknow, Uttar
Pradesh, India

Vikas Trivedi
Professor, Department of
Orthopaedics, Era's Lucknow
Medical College, Lucknow, Uttar
Pradesh, India

Dr. Priyank Sahoo
Department of Orthopaedics,
Era's Lucknow Medical College,
Lucknow, Uttar Pradesh, India

Imran Shakeel Khan
Department of Orthopaedics,
Era's Lucknow Medical College,
Lucknow, Uttar Pradesh, India

Dr. Rahul Dwivedi
Department of Orthopaedics,
Era's Lucknow Medical College,
Lucknow, Uttar Pradesh, India

Dr. Afroz Ahmed Khan
Assistant Professor, Department
of Orthopedics, Era's Lucknow
Medical College and Hospital,
Uttar Pradesh, India

Corresponding Author:
Dr. Priyank Sahoo
Department of Orthopaedics,
Era's Lucknow Medical College,
Lucknow, Uttar Pradesh, India

Morphological and mechanical properties of bone tissues

Dr. AN Mishra, Dr. Shakeel A Qidwai, Vikas Trivedi, Dr. Priyank Sahoo, Imran Shakeel Khan, Dr. Rahul Dwivedi and Dr. Afroz Ahmed Khan

DOI: <https://doi.org/10.22271/ortho.2019.v5.i4l.1749>

Abstract

Introduction: Adult human skeletal system consists of 206 bones and this system gives the human body its shape, supports it, and helps in movements. These bones are made of living bones tissues which replenish throughout the lifetime of an individual. There are different bone diseases associated to these bone tissues like osteoporosis, low bone density, osteogenesis imperfecta, and Paget's disease of bones which happen when these bone tissues synthesis is not normal, and can cause fracture. The most common bone disease is osteoporosis which causes bones to become less dense and more fragile. It affects the entire skeletal system and causes fracture in hips, wrists, ankles, and spine commonly.

Methodology:

CT Scanning
Three calcaneus bone samples were scanned using micro CT (SkyScan 1172, Aartslaar, Belgium) at the voxel size of 17.41 μm , rotating at increments of 0.7° for 180°, and the data was stored in numbered 16bit high resolution grayscale images.

Results: The analysis of bone properties has not been limited to mechanical testing only. With the development of computer tomography techniques and finite element modelling software, the researchers have started using simulations to study bone morphology and properties. The previous studies indicate that not much has been done to study the fracture mechanism of calcaneal trabeculae. So, this study was designed to conduct compression test on sections of calcaneal trabeculae and compare it with the available results.

Conclusion: The study focuses on the mechanical properties of trabecular bone in compression. The main purpose of the study is investigating the factors which could influence the mechanical properties of the trabecular bone.

Summary: The human skeletal system suffers from number of diseases like osteoporosis, osteoarthritis, and Paget's disease which impair its function and cause discomfort and fracture to patients. The study of bone properties have helped in treating a variety of bone diseases. This study involved non-destructive finite element analysis of calcaneal trabecular bone specimens under compressive loading. Three calcaneal trabecular bone specimens were scanned using micro CT and 3D models were reconstructed using the image data. The reconstructed models were assigned material heterogeneous properties based on grayscale values from the images. These models were converted to FE models with a variety of mesh coarseness and analysed, and the best models were used for further finite element analysis. The results were compared with previous studies and matched subject to certain errors. It was concluded that mesh parameters affect the quality of finite element simulation and the heterogeneous bone material properties caused non-uniform deformation in the trabeculae structure.

Keywords: Osteoporosis, calcaneum, CT scan, model

Introduction

Background

Adult human skeletal system consists of 206 bones and this system gives the human body its shape, supports it, and helps in movements. These bones are made of living bones tissues which replenish throughout the lifetime of an individual. There are different bone diseases associated to these bone tissues like osteoporosis, low bone density, osteogenesis imperfecta, and Paget's disease of bones which happen when these bone tissues synthesis is not normal, and can cause fracture. The most common bone disease is osteoporosis which causes bones to become less dense and more fragile. It affects the entire skeletal system and causes fracture in hips, wrists, ankles, and spine commonly.

According to NHS, it is caused due to various factors which include age, genetics, gender, diet, lack of exercise, hormonal disorder, heavy drinking or smoking, and parental history. The fractures caused by bone diseases like osteoporosis affects around 1.5 million people annually [1]. In 2010, 22 million women and 5.5 million men were estimated to have osteoporosis in the EU; and 3.5 million new fragility fractures were sustained, comprising 620,000 hip fractures, 520,000 vertebral fractures, 560,000 forearm fractures and 1,800,000 other fractures [2]. In USA, aging of population is expected to increase the cases of osteoporosis among individual over the age of 50 from 10 million cases in 2002 to 12 million in 2010, and to nearly 14 million cases by 2020 [3]. Researches show that different morphological properties correspond to the mechanical properties of the bones and this helps us deal with disease like osteoporosis which affects the morphometric properties of the bones and weaken them. But, different types of bones have different morphological and mechanical properties and bones adapt to their mechanical environment according to Wolff's Law [4]. So, it is essential to study bone tissue samples from different parts of the body as these tissues have different mechanical and morphometric properties.

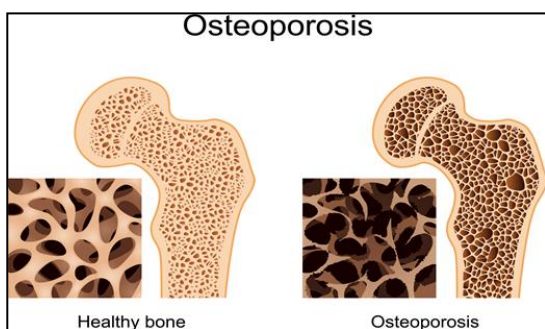


Fig 1: Trabeculae of healthy bone and osteoporotic bone [5]

Aims and objectives

This project aimed at studying the different mechanical and morphological properties of three different specimens of calcaneus bones by non-destructive analysis using micro CT, and Finite Element modelling.

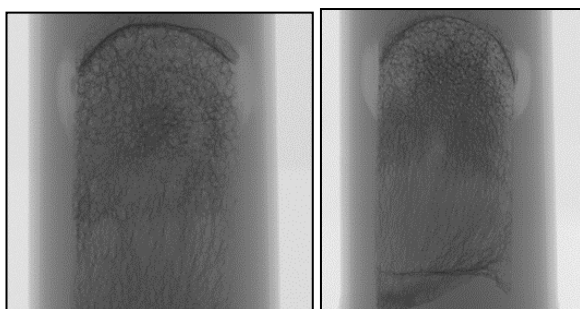


Fig 2: R711

Fig 3 R715

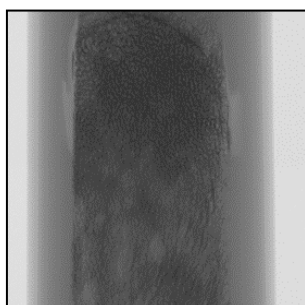


Fig 4 R737

The above three different calcaneus bone samples were scanned using micro CT. The different stacks of images obtained for the three different samples were imported into Scan IP software. The stacks of images were then converted into 3D models using segmentation tools and various filters. The 3D models were converted into FE models and exported into ABAQUS. The models were then simulated under compressional loading and various mechanical parameters were measured, and the results were compared to previous findings.

The following were the objectives to achieve the aim

- To obtain background information regarding the project and understand the context and importance of this study in dealing with bone diseases.
- To learn about microstructure of different bone tissues from different parts of the body and analyse the differences between them.
- To obtain and segment micro CT images, and generate FE modulus.
- To familiarise using Scan IP and ABAQUS and import and create 3D models of the bone samples provided and perform mechanical tests using ABAQUS.
- To analyse the results obtained from finite element analysis.
- To investigate how microstructure in bone tissues affect the mechanical properties of bone specimen.

Literature review

Introduction

The mechanical properties of human trabeculae, the relation between bone volume and large strain compressive behaviour of trabeculae, the alignment of trabeculae along the direction of continuous strain also known as Wolff's law, and the use of computer tomography and finite element technology have been widely researched and documented.

Calcaneus bone is the heel bone in human skeletal system and part of tarsus constituting the heel. This is the largest bone among the tarsals and also the largest bone of the foot.

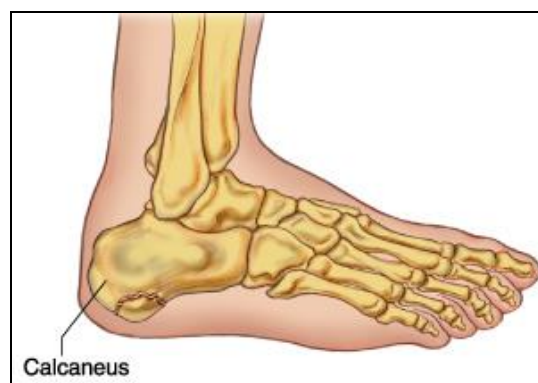


Fig 5: Calcenus bone (6)

Fractures in calcaneus bone can be caused in high energy event, like a car crash, or a fall from a height landing on the heels. This causes it to widen or shorten. Due to mostly being caused by fall from a height, this fracture came to be known as Lover's fracture and Don Juan's fracture after the sixteenth century fictional libertine womanizer.

Review of previous studies

Research on calcaneal fractures and treatments

Yoganandan *et al.* [7] designed a study to derive probability

distribution to represent human calcaneal tolerances under impact loading like in a vehicle collision or fall from a height. The calcaneal specimens were dynamically loaded in plantar surface once using mini-sled pendulum equipment. There were 14 cases of no fracture and 12 cases of calcaneal fracture. The mean fracture force was 7802 N while the probability of calcaneal fracture showed that 6.2 kN force corresponded to 50% probability of calcaneal fracture. In another similar study conducted by Gallenberger *et al.* [8], 60 pendulum impacts to the plantar surface of 15 lower limb PMHS specimens were conducted to study the difference between fracture forces of dorsiflexed specimen and neutral specimen. 19 impacts were conducted with specimen positioned initially at 20° of dorsiflexion while the rest were conducted at neutral positioning. The results indicated that dorsiflexed specimen had 50% injury probability at 7900 N which was higher than that of neutral specimen at 6800 N.

Further studies were conducted for the treatment of calcaneal fractures. In a study conducted by Zhang *et al.* [9], the minimally-invasive lateral approach for displaced intra-articular calcaneal fracture treatment and the conventional sinus tarsi approach were studied and compared. The results indicated minimally-invasive approach had lower postoperative complications than the sinus tarsi approach and had similar functional outcomes. Schubert *et al.* [10] conducted a study involving 24 cases of minimally invasive, open reduction, and internal fixation of intra-articular calcaneal fractures. The results showed that minimally invasively approach improved radiographic parameters and had minimal wound complications. There were no soft-tissue complications and none of the 18 patients progressed to subtalar fusion for over a year.

Arbenz *et al.* [14], the effects of smoothing on the finite element solution were studied. The models were analysed every time after applying a smoothing step till 28 steps. The results indicated that smoothing resulted in large subjective improvement of visualisation and that the conditions of stiffness matrix don't vary too much as long as the model is not distorted too severely. Increased smoothing led to longer simulation time as the stiffness matrix must be computed for each individual element and smoothing increased the number of elements. In a lecture delivered by Wang [15], the different types of filters in ScanIP were analysed. The differences between Mean, Median, and Recursive Gaussian filter were mentioned.

Use of finite element modelling

Finite element analysis has been proven to accurately simulate fracture mechanisms. With the advent of technology and improvement in finite element analysis software, this technique of non-destructive analysis is becoming very popular for research studies. In a study conducted by Chevalier *et al.* [16], reconstructions of micro-CT and finite element analysis of trabeculae was combined with physical measurement of volume fraction, and mechanical tests for appropriate validation of the method. The results indicated that the results of mechanical tests matched the finite element predictions. Huang *et al.* [17] studied the mechanism of

calcaneal fracture by establishing 3D finite element models of calcaneus. They scanned the calcaneus of a normal person and converted the images into a 3D finite element model with 1,496 elements which was loaded axially with 500 N in neutral position and 20° dorsiflexion. The results showed that the fracture line passed through the facet of talocalcaneal joint from lateral to post medial side in neutral position, and through the calcaneus body to post spinula joint in dorsiflexion. However, this study was limited due to technological constraints.

In a recent study by Wong *et al.* [18], the influence of foot impact on the risk of calcaneus fracture was assessed via finite element modelling. A 3D finite element model of foot and ankle was constructed from MRI images of a female aged 28, and loaded with 7kg passive impact through foot plate. The impact velocities simulated were from 2.0 to 7.0 ms⁻¹ with 1.0 ms⁻¹ interval. The results showed that at 5 ms⁻¹ impact velocity, the maximum Von Mises stress and Tresca stress for calcaneus were 3.21 MPa and 3.46MPa respectively, and the peak stresses were distributed around talocalcaneal articulation which corresponds to the common fracture sites.

Conclusion

The analysis of bone properties has not been limited to mechanical testing only. With the development of computer tomography techniques and finite element modelling software, the researchers have started using simulations to study bone morphology and properties. The previous studies indicate that not much has been done to study the fracture mechanism of calcaneal trabeculae. So, this study was designed to conduct compression test on sections of calcaneal trabeculae and compare it with the available results [18]. Also, careful reconstruction of micro CT images was done to have the best possible simulation for compression test. This test also accounts for the fact that trabeculae properties are heterotropic and anisotropic as found by the studies conducted by Boyde *et al.* [21].

Methodology

CT Scanning

Three calcaneus bone samples were scanned using microCT (SkyScan 1172, Aartslaar, Belgium) at the voxel size of 17.41 µm, rotating at increments of 0.7° for 180°, and the data was stored in numbered 16bit high resolution grayscale images.

Image reconstruction in Scan IP

Reconstruction of R711

The first stack of images was R711. Five different models were created using different approaches and the best model was selected for FE modelling.

- **Model 1** – The images 151 to 440 were imported into the ScanIP software so that the height of the stack was ~5mm. A section of 10mm X 10mm was taken near the centre of the images. To remove noise, 2 pixels are skipped on all three orientations.

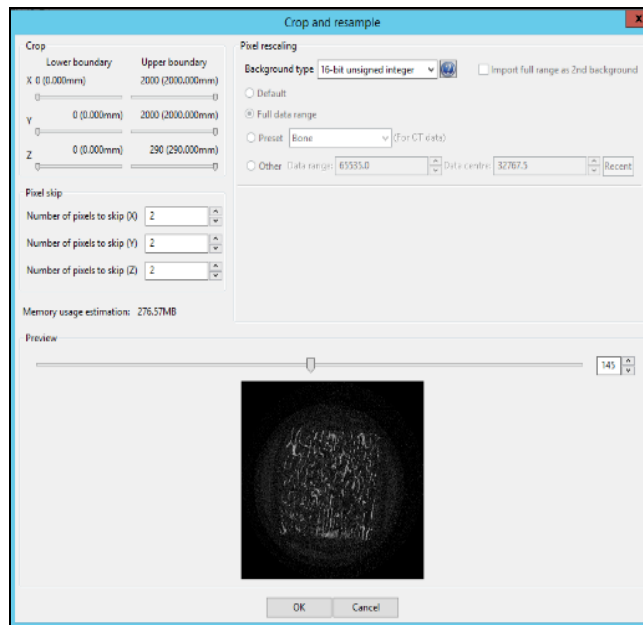


Fig 7: Custom Pixel skipping

The trabeculae were segmented from the background using ‘Threshold’ tool with lower limit set at 20512 and the upper limit at 50921.

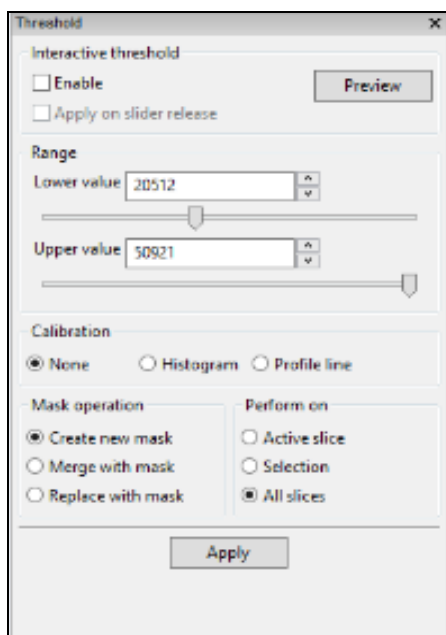


Fig 8: Thresholding

Smoothing was done using ‘Recursive Gaussian’ filter with ‘Binarisation’ and Gaussian sigma value of 0.6 in all directions. Further noise and unwanted islands were removed using ‘Island Removal’ tool with 250 voxels as island threshold size.

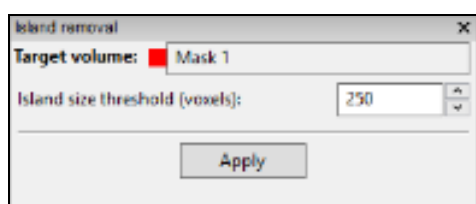


Fig 9: Island removal

- **Model 2:** The second model was created using the same set of steps as the first model, but smoothing was done using only ‘Binarisation’ filter.
- **Model 3:** Same set of steps were used for generating Model 3, but smoothing was done using ‘Median’ filter, first on the background with 1 pixel as neighbourhood radius on all three orientations and then on the mask.
- **Model 4:** The same stack of images were used to generate model 4, with the same dimensions. However, the default pixel skipping setting for Scan IP software was used which skipped only 1 pixel in all orientations.

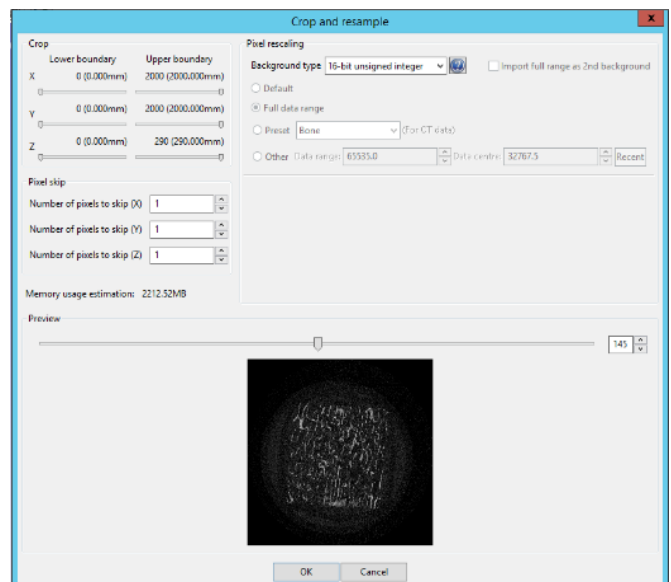


Fig 10: Default pixel skipping

The trabeculae were segmented from the background using ‘Threshold’ tool with lower limit set at 20512 and the upper limit at 50921. Smoothing was done using the ‘Median’ filter, first on the background with 3 pixels as neighbourhood radius, and then on the mask with pixel as neighbourhood radius.

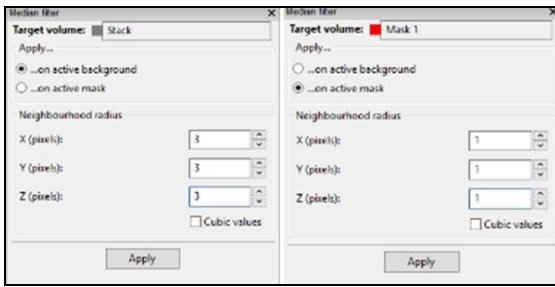


Fig 11: Median filter

Model 5: The images 1151 to 1440 were imported and the other steps were kept same as that used to generate model 4. However, further smoothing was done using ‘Recursive Gaussian’ with ‘Binarisation’ and low Gaussian sigma value of 1.2 pixels in all three orientations to minimise feature loss from high Gaussian sigma values. This model was chosen for FE model generation.

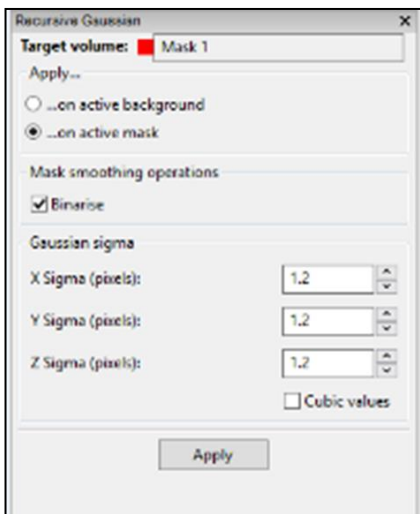


Fig 12: Recursive Gaussian filter.

Result

Image reconstruction in scan IP

Reconstruction of R711

- Model 1:** The model generated was very smooth and had no noise, however a lot of the original features were removed due to excessive smoothing (recursive Gaussian) and skipping 2 pixels when importing images. The model had 2,481,600 triangles and was 34.17 MB large.

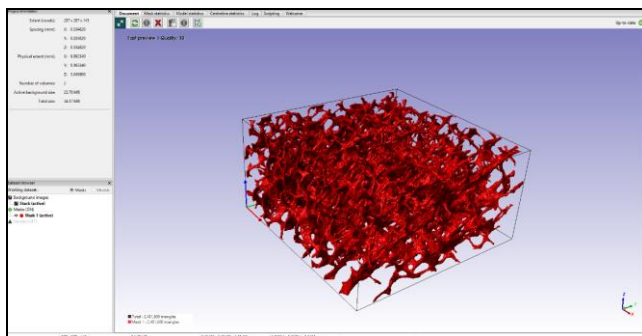


Fig 21: R711 Model 1

- Model 2:** The model generated was coarser compared to model 1 and had a bit of noise because only ‘Binarisation’ was used for smoothing, however a lot of

the original features were removed due to skipping 2 pixels when importing images. The model had 2,607,816 triangles and was 34.17 MB large.

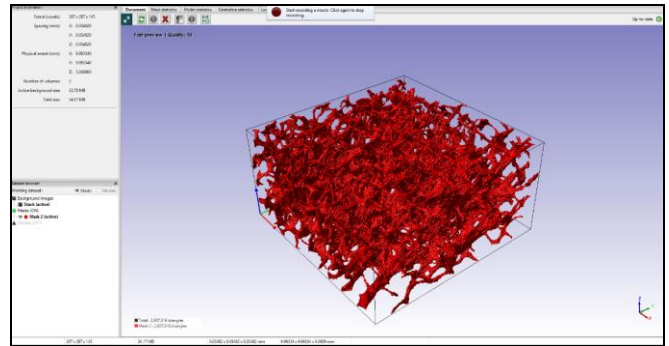


Fig 22: R711 Model 2

- Model 3:** The model generated was closer to real structure of trabeculae, coarser than 1 and 2 as only ‘Median’ filter was used for smoothing. This model still removed a lot of the features due to skipping 2 pixels when importing images. The model had 2,152,280 triangles and was 34.17MB large.

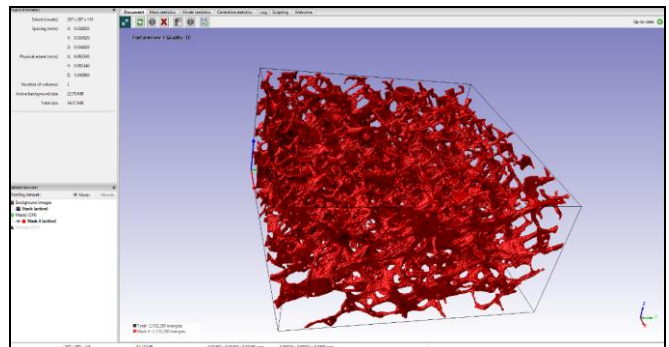


Fig 23: R711 Model 3

- Model 4:** The model generated is closer to real structure of trabeculae and has preserved the original features due to default pixel settings. The model is fairly smooth due to use of ‘Median’ filter, and has a bit of noise due to no ‘Binarisation’. The model has 9,976,004 triangles and is 273.37 MB large.

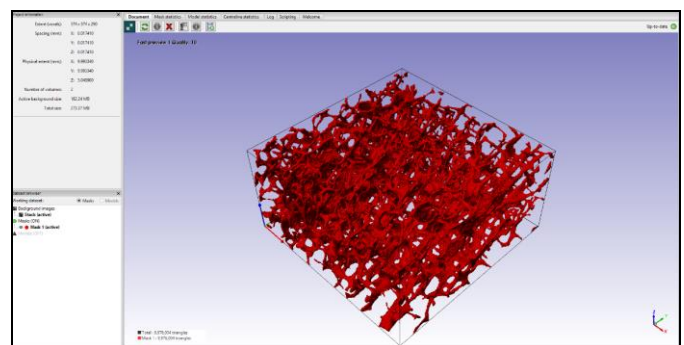


Fig 24: R711 Model 4

- Model 5:** The model generated is very smooth due to added ‘Recursive Gaussian’ filter, has no noise, and has preserved most of its features due to low Gaussian sigma value, and is the best model to use for simulation. The model has 12,679,944 triangles and is 273.37 MB large.

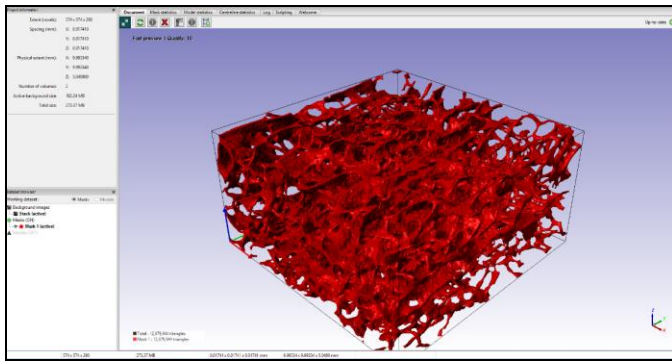


Fig 25: R711 Model 5

Reconstruction of R715

- Model 1:** The model generated used the steps used for generating Model 4 of R711 and has preserved the original features due to default pixel settings. The model is fairly smooth due to use of 'Median' filter, and has a bit of noise due to no 'Binarisation'. The model has 9,930,280 triangles and is 273.37 MB large.

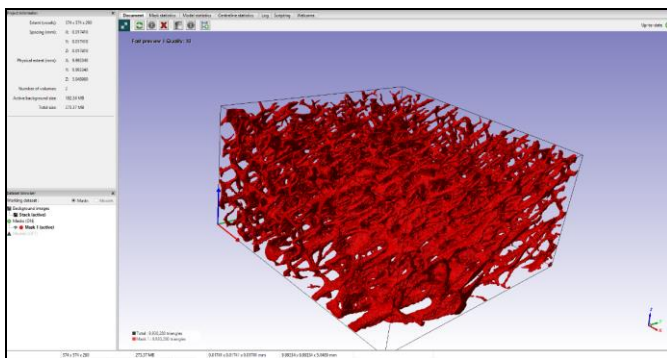


Fig 26: R715 Model 1

- Model 2:** The model generated has 14,379,520 triangles and is 273.37 MB large. It has more number of triangles due to added 'Recursive Gaussian' filter and is the model used to generate FE model for R715.

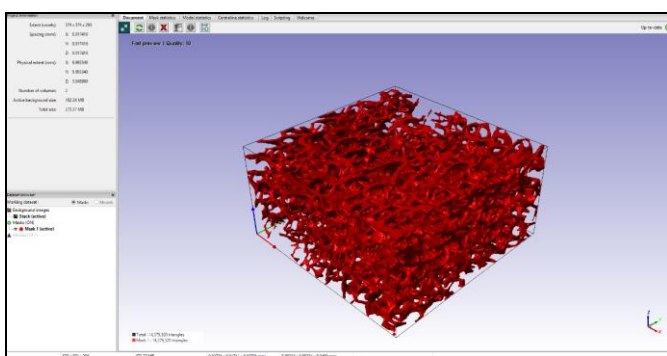


Fig 27: R715 Model 2

Reconstruction of R737

- Model 1:** The model generated used the steps used for generating Model 4 of R711 and is fairly smooth due to use of 'Median' filter, and has a bit of noise due to no 'Binarisation'.

- The trabeculae density is the highest in this stack of images. Hence, the model has 28,103,924 triangles and is 273.37 MB large.

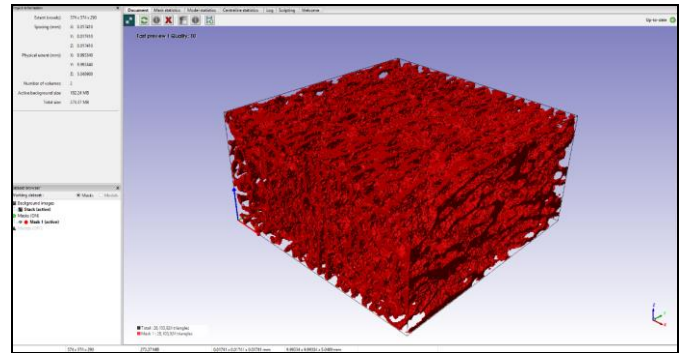


Fig 28: R737 Model 1

- Model 2:** The model generated has 23,337,824 triangles and is 273.37 MB large. This model is used to generate FE model for R737 because it is smoother than Model 1 and has no noise.

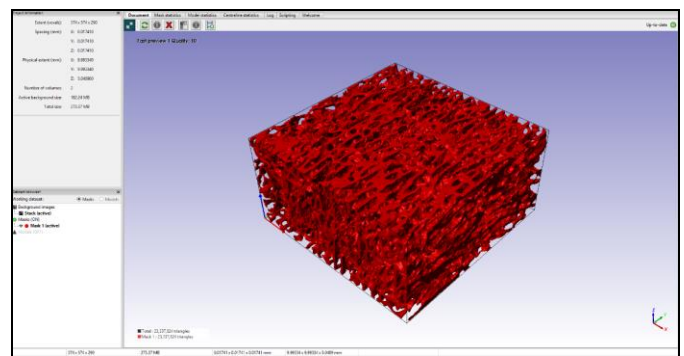


Fig 29: R737 Model 2

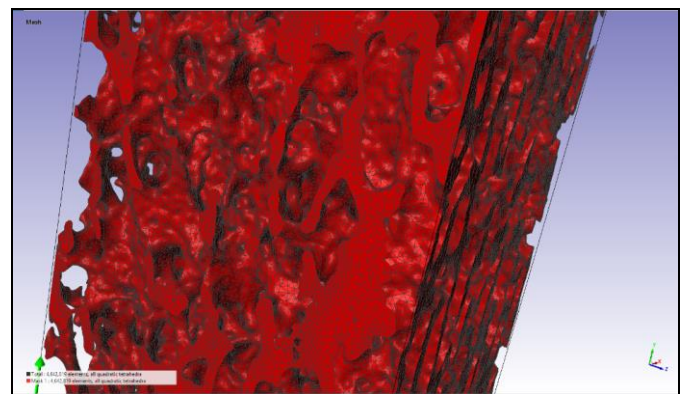


Fig 30: Mesh Quality R737

The generated mesh was of very high quality, with no errors, and less than 1% distorted elements for each model apart from R737:

- R711:** For the first model, the number of distorted elements was 9,218 which were 0.59% of total elements. For the second model, the number of distorted elements was 7,747 which were 0.39% of total elements. There were 2 unconnected regions in both models.

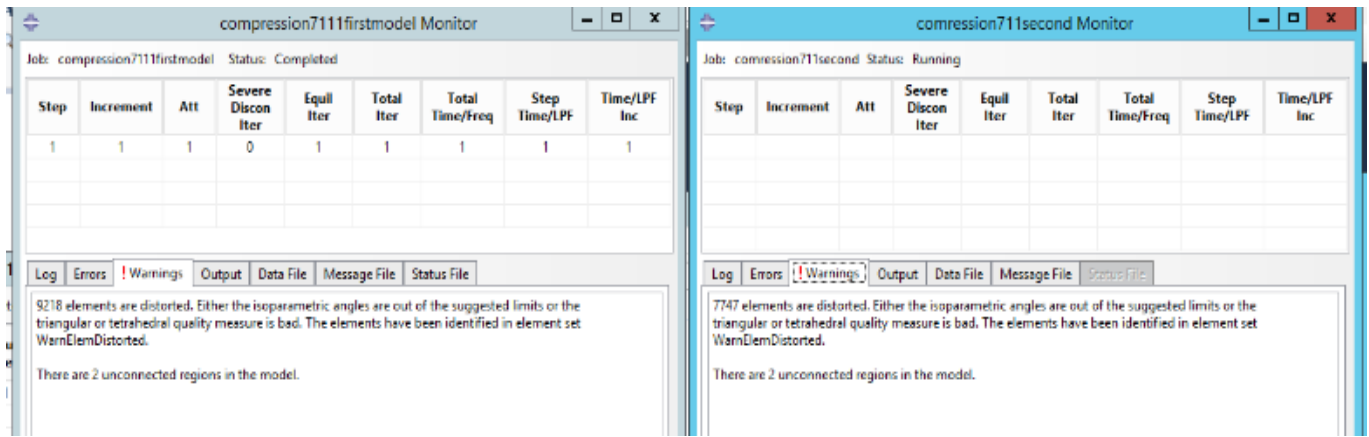


Fig 31: R711 - number of distorted elements

- **R715:** There were 12,021 distorted elements which were regions. 0.74% of total elements. The model had 31 unconnected

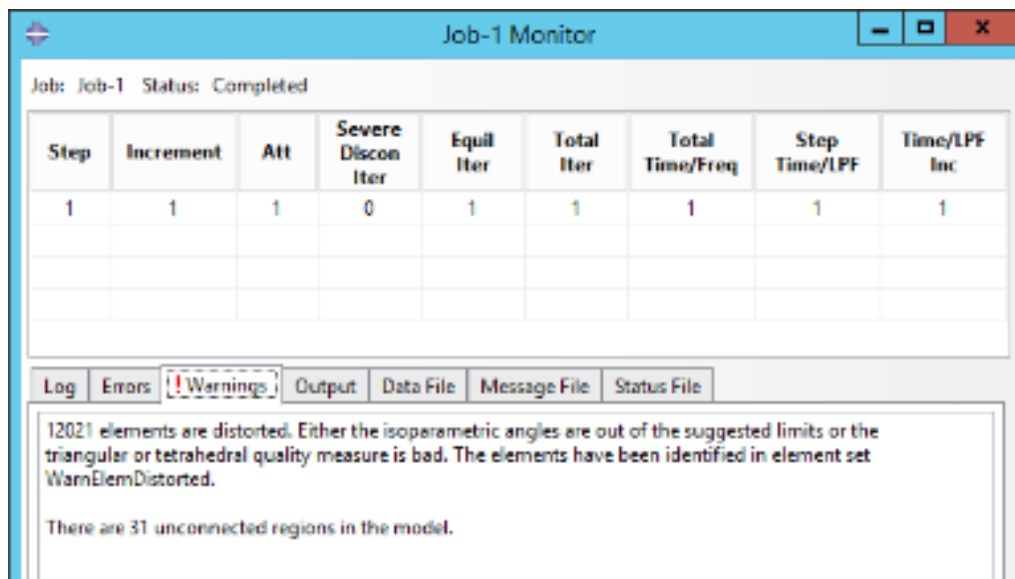


Fig 32: R715 - number of distorted elements

- **R737** – There were 367,298 distorted elements which were regions. 7.91% of total elements. The model had 3 unconnected

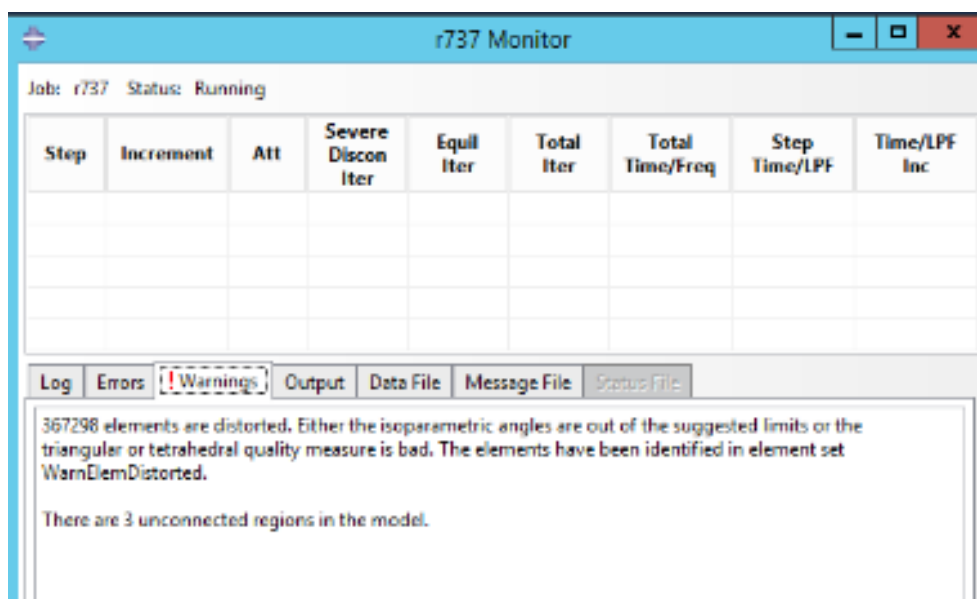


Fig 33: R737 number of distorted elements

R711

- **Model 1** – The first model had a maximum value of Von Mises stress of 4.12 MPa.

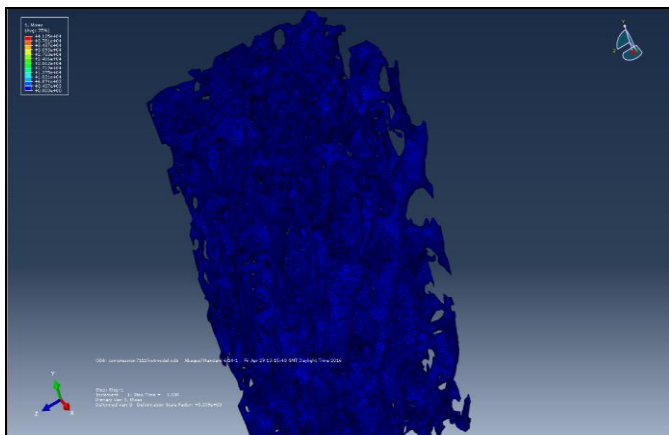


Fig 34: R711 Model 1 - Von Mises stress distribution

The peak stresses were distributed around the nodes which had the material properties of least Young’s modulus. These nodes had the least mass density as well.

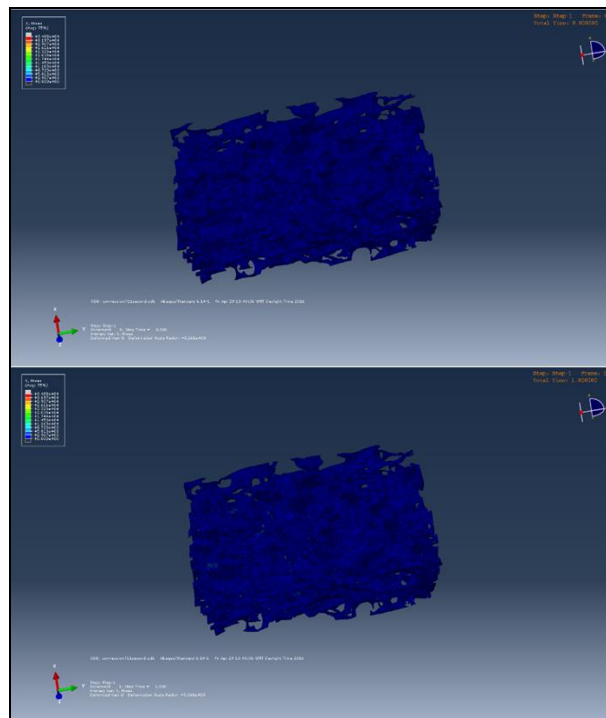


Fig 37: Animation - Time History

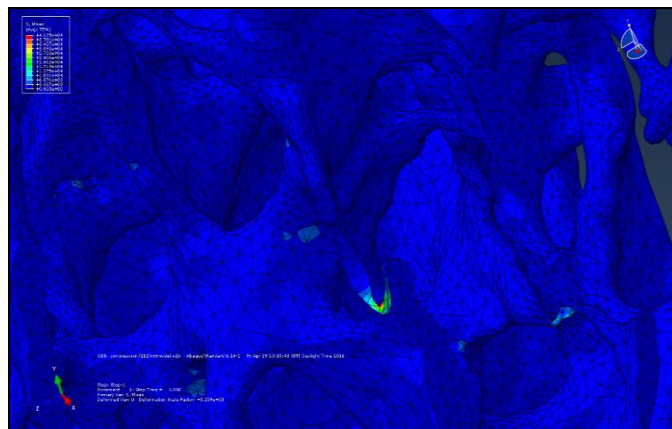


Fig 35: R711 Model 1 - Enlarged Von Mises

The maximum deformation occurred along the nodes with high stress distribution.

- **Model 2** – The second model had a maximum value of Von Mises stress of 3.48 MPa.

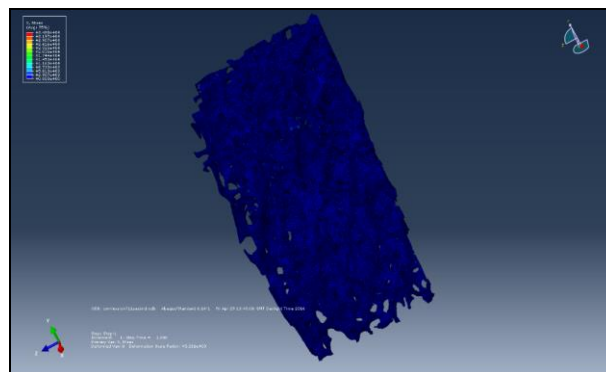


Fig 38: R711 Model 2 - Von Mises stress distribution

Like the first model, the peak stresses were distributed around the nodes which had the material properties of least Young’s modulus. These nodes had the least mass density as well. Also, the maximum deformation occurred at the nodes with high stress distribution.

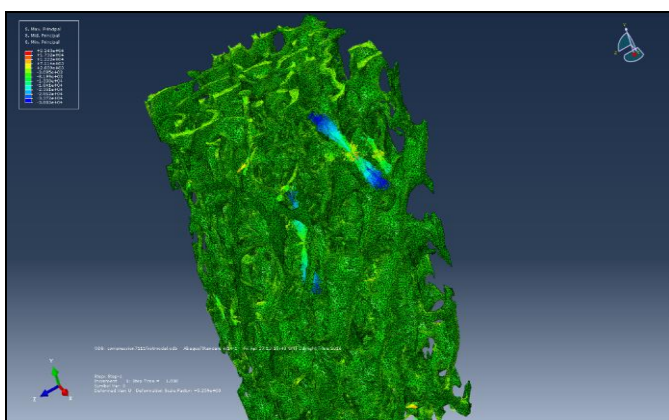


Figure 36: R711 Model 1 – Deformation

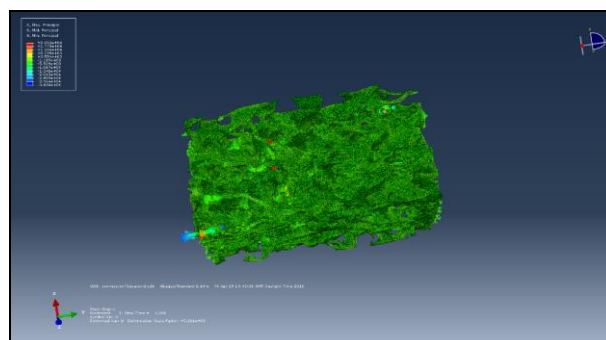


Fig 39: R711 Model 2 - Deformation

The ‘Animation’ tool showed the deformation of the model over the extent of compression test.

R715

The maximum value of Von Mises stress was 5.53 MPa.

Discussion**Finite Element Modelling****Image reconstruction in Scan IP**

Two general approaches were used to generate masks for R711 in Scan IP. The first one involved using pixel skipping to reduce the size of generated mask while the other approach did not skip pixel. It was observed that pixel skipping reduced the number of elements in the mask and hence the size of the generated model. However, visual examination showed that skipping pixel also got rid of the features of the model. The smaller models would have taken lesser time to analyse due to the delicate nature of trabeculae analysis, it was necessary to preserve as much of the original features as possible.

Another important step was to reduce noise in the model as much as possible. Noise filtering, if done incorrectly, would have resulted in a higher percentage of distorted elements and unconnected region in the generated mesh. So, a combination of filters was used to reduce the noise. Each model used for generating mesh had a combination of median filter used both in the background and the mask, island removal filter, and recursive Gaussian filter with low Gaussian sigma value. The median filter used in the background helped in removing excessive noise which helped in reducing the time taken by island removal tool. If used alone island removal tool took longer to remove the excessive noise. The low Gaussian sigma value insured preservation of model features along with high quality smoothing.

Limitations and future work

The study conducted non-destructive analysis of calcaneal bone samples. There was no physical test conducted. So, mechanical testing of bone samples need to be conducted along with FE analysis to better study the properties of bone tissues.

Also, there were software constraints which allowed only static analysis of the model. So, in future dynamic analysis with impact loading should be conducted while finite element simulation.

Conclusion

The study focuses on the mechanical properties of trabecular bone in compression. The main purpose of the study is investigating the factors which could influence the mechanical properties of the trabecular bone. Before the mechanical test, twelve cylindrical bone samples were prepared by cutting and drilling the left medial femur condyle of an 18-month-old cow. Then, these bone samples were embedded in the PMMA resin with the assisting of a new design sample holder. Some problems were met during the calibrating process, but had been solved by changing the mounting method of the sample holder. The unconfined compression test was performed on 12 cylindrical bone samples by an electrical-dynamic test instrument. The engineering stress-strain curves were plotted and analysed. For the finite element analysis, a human proximal femur was scanned by the μ CT scanner to obtain the high resolution CT imagines. Then, thousands of CT imagines were segmented and generated to 3D FE model. To obtain the most reasonable mesh density, a mesh independent study was performed before the formal simulation. Then, a same simulation was repeated for several times with different tissue modulus to find out the relationship between the Young's modulus of the

bone model and the modulus of bone tissue. Two different settings of boundary conditions were also applied in the FE analysis, and the results of the two boundary conditions were generated and compared. All experiment and simulation results were shown in the form of figures and table, especially some comparison figure were made elaborately. The three basic conditions of misalignment was diagrammatized and introduced, the mechanical properties of trabecular bone and porous materials were compared, the influences caused by the different boundary conditions for the FE model were analysed, the collapse process of trabecular was discussed and the reliability of FE analysis was verified by comparing the results from the previous studies. The study concluded that the misaligned sample with better mechanical behaviour, the mechanical properties of trabecular bone is similar with that of porous materials, apparent Young's modulus is proportional to the tissue modulus and the simulation results are sensitive to the boundary conditions.

References

1. Riggs BL, Melton LJ. The worldwide problem of osteoporosis: Insights afforded by epidemiology. *Bone*. 1995; 17:505S-511S.
2. Svedbom A, Hernlund E, Ivergård M, Compston J, Cooper C, Stenmark J, *et al.* Osteoporosis in the European Union- a compendium of country specific reports: *Archives of osteoporosis*. 2013; 8:1-218.
3. National Osteoporosis Foundation. America's bone health: The state of osteoporosis and low bone mass in our nation. Washington (DC): National Osteoporosis Foundation, 2002.
4. Pearson OM, Lieberman DE. The Aging of Wolff's "Law": Ontogeny and Responses to Mechanical Loading in Cortical Bone: *American journal of physical anthropology*. 2004; 39S:63-99.
5. Lee L. Osteoporosis and Fracture prevention, 2013. Available at: https://prezi.com/w_2904_hhmr9/osteoporosis-and-fracture-prevention/
6. Medical disability advisor. Nodate. Fracture, Calcaneus. Available at: http://www.mdguidelines.com/images/illustrations/fr_calca.jpg
7. Yoganandan N, Pintar FA, Gennarelli TA, Seipel R, Marks R. Biomechanical Tolerances of Calcaneal Fractures: Annual Proceedings / Association for the Advancement of Automotive Medicine. 1999; 43:345-356.
8. Gallenberger K, Yoganandan N, Pintar F. Biomechanics of foot/ankle trauma with variable energy impacts: *Annals of Advances in Automotive Medicine*. 2013; 57:123-132.
9. Zhang T, Su Y, Chen W, Zhang Q, Wu Z, Zhang Y. Displaced intra-articular calcaneal fractures treated in a minimally invasive fashion' longitudinal approach versus sinus tarsi approach: *The Journal of Bone and Joint Surgery, American Volume*. 2014; 96(4):302-309.
10. Schubert JM, Cobb MD, Talarico RH. Minimally invasive arthroscopic-assisted reduction with percutaneous fixation in the management of intra-articular calcaneal fractures, a review of 24 cases: *Journal of Foot and Ankle Surgery*. 2009; 48(3):315-322.
11. Røhl L, Larsen E, Linde F, Odgaard A, Jørgensen J. Tensile and compressive properties of cancellous bone: *Journal of Biomechanics*. 1991; 24(12):1143-1149.
12. Öhman C, Baleani M, Perilli E, Dall'ara E, Tassani S, Baruffaldi F, *et al.* Mechanical testing of cancellous bone

- from the femoral head: Experimental errors due to off-axis measurements: *Journal of Biomechanics*. 2007; 40(11):2426-2433.
13. Razmkhaha O, Ghasemnejad H. Development and validation of 3D finite element model based on CT images: *North Atlantic University Union Journal*. 2013; 1:145-147.
 14. Arbenz P, Flaig C. On smoothing surfaces in voxel based finite element analysis of trabecular bone: Large-scale scientific computing, 6th International Conference, Sozopol, Bulgaria, 2007.
 15. Wang Y, Image filtering: Noise Removal Sharpening, Deblurring: EE3414- Multimedia Communication Systems -1. Polytechnic University, Brooklyn, 2006.
 16. Chevalier Y, Pahr D, Allmer H, Charlebois M, Zysset P. Validation of a voxel-based FE method for prediction of the uniaxial apparent modulus of human trabecular bone using macroscopic mechanical tests and nanoindentation: *Journal of biomechanics*. 2007; 40(15):33-40.
 17. Huang ZH, Li J, Chen RQ, Du JW, Zhang JX. Three-dimensional finite element analysis of calcaneal fractures: *Zhongguo Gu Shang*. 2012; 25:97-101.
 18. Wong Dw, Niu W, Wang Y, Zhangm. Finite element analysis of foot and ankle impact injury: *PloS One*. 2016; 11:e0154435.
 19. Simpleware Scan IP, +Scan FE, and +Scan CAD Tutorial Guide. Exeter, UK, 2010.
 20. Dassault Systèmes. Abaqus 6.12 Getting Started with Abaqus: Interactive Edition. Providence, RI, USA, 2012.
 21. Boyde A, Elliot JC, Jones SJ. Stereology and histogram analysis of backscattered electron images: Age Changes in Bone: *Bon*. 1993; 14(3):205-210.